Available online at www.sciencedirect.com
SCIENCE DIRECT®
European Journal of Mechanics B/Fluids 24 (2005) 572–585

The dynamics of a moving sheet of liquid, part II: experiments

M. Gilio, F. Al-Bender *, J.-P. Kruth

Katholieke Universiteit Leuven, Department of Mechanical Engineering, Celestijnenlaan 300B, 3001 Heverlee, Belgium

Received 28 January 2004; received in revised form 9 December 2004; accepted 13 December 2004

Available online 10 February 2005

Abstract

The transient response of a planar liquid sheet, subjected to an acceleration in a direction normal to its plane of flow is investigated both experimentally and numerically, for various acceleration trajectories. Experiments were performed by video recording the sheet during acceleration, and measuring its deflection from the captured frames. Experimental data shows a very weak dependence of the sheet's response's settling time on the acceleration trajectory parameters. Based on the equations of motion derived in part I, a computational model is developed to simulate the transient response. Preliminary computations neglect the influence of air surrounding the sheet, and yield only qualitative agreement with experiments. The air, trapped between sheet and shields, is assumed to exert a damping influence on the sheet's response. The computational model is modified by introducing a nonlinear damping element, which is empirically identified. Solutions of this extended model show improved agreement with experiments.

Keywords: Liquid sheet; Transient; Deflection; Acceleration

1. Introduction

In a previous paper (part I) a coating method was described that made use of a translating planar liquid sheet to coat a layer of liquid. This coating method is used in a manufacturing process called stereolithography. A coating die from which a liquid sheet emanates is repetitively moved over a liquid pool onto which new liquid layers are coated. Products are built in this pool by selectively curing the liquid layer after layer. A detailed description of the application may be found in part I.

When the coating die is set into motion, it is accelerated to a given coating speed, V_C. This causes an important transient response of the sheet, in which the sheet deflects out of its plane of flow. This part II paper provides experimental results of the transient response of a liquid sheet when the coating die, from which the sheet emanates, is subjected to a time-dependent acceleration. The liquid sheet falls vertically under the influence of gravity, and the acceleration considered is perpendicular to the plane of flow. The investigation is carried out because the transient response needs to have dissipated before a liquid layer may actually be coated.

* Corresponding author.
E-mail address: farid.al-bender@mech.kuleuven.ac.be (F. Al-Bender).

0997-7546/$ – see front matter
doi:10.1016/j.euromechflu.2004.12.002

Nomenclature

AL	acceleration length	V_C	coating speed
a_D	acceleration of the coating die	v	normal velocity component
a_{peak}	peak acceleration	ε	slenderness ratio ($T_0 L^{-1}$)
f	normal velocity of the sheet's centre line	ζ	damping ratio ($c(2\sqrt{mk})^{-1}$)
g	gravitational acceleration	θ	angle of the sheet's centre line with the vertical axis
L	sheet length		
$\ell_{\max}$	maximal sheet deflection at lower end	κ	curvature of the sheet's centre line ($\partial\theta/\partial s$)
p^g	gas pressure	μ	dynamic viscosity
Q	flow rate per unit sheet width	ρ	liquid density
Re	Reynolds number ($\rho u_s T_0 \mu^{-1}$)	σ	surface tension
T	sheet thickness	τ_{90}	time for the sheet's response to decay to 10% of $\ell_{\max}$
T_0	initial sheet thickness (at die exit)		
u	streamwise velocity	τ_{peak}	time to peak acceleration
u_0	initial mean streamwise velocity (at die outlet)	ω_n	natural frequency ($\sqrt{km^{-1}}$)
u_s	streamwise velocity scale ($\sqrt{gL}$)		

The experimental results are compared with solutions obtained from equations of motion that have been derived in part I of this series of papers. The authors are presently not aware of any previous study about the transient dynamics of liquid sheets subjected to an acceleration of the die from which they emanate. However, quite extensive research on *stationary* (i.e. not translating) liquid sheets is found in literature. Topics mostly concern sheet stability [1–3] and coating practice [4,5]. Noteworthy at this point is the work of Weinstein et al. [6] and Clarke et al. [7], who investigated the dynamic response of two-dimensional, inviscid liquid sheets subject to small, high frequency disturbances in ambient pressure. The pressure disturbances were generated using an electrostatic field perpendicular to the liquid surface. The frequency of the applied disturbances ranged between 40 and 110 Hz. The experimental results were compared to solutions of the linearised time-dependent potential flow equations, showing good agreement. These findings are however of limited use for the present work, because of the order of magnitude of the disturbances, the different nature of the exciting force, and the viscid properties of the liquid under investigation.

The present work was undertaken in order to (i) investigate to which extent the transient response was affected by the acceleration trajectory that was applied to the coating die, and (ii) to identify additional parameters influencing the response. The goal is to have the transient response decay as fast as possible.

The experiments are discussed first. The results of numerical computations are shown afterwards. The paper starts with an outline of the experimental set-up and procedure, followed by a description of the experiments that have been undertaken to quantify the transient response of the sheet. Next, the results of numerical simulations, based upon the equations derived in part I, are presented. Comparison of experiments with computations makes clear that the shielding of the sheet is an important element. However, modelling the influence of shielding the sheet, on the transient response is very difficult. It is shown in this paper, that the shielding causes a damping effect on the sheet's transient response. An empirically determined, nonlinear damping term was added to the equation governing the sheet's out-of-plane deflection. Solutions of this extended model with added damping show satisfactory agreement with experiments.

2. Experimental set-up and procedure

The experiments consisted in imparting a given acceleration trajectory to the coating die, from which the sheet emanates. The planar sheet experienced a transient response during which an out-of-plane deflection was observed. The deflection was recorded by a video camera and analysed to extract quantitative data.

Fig. 1 depicts a front view of the test set-up, that was used for the experiments. A liquid sheet is extruded out of a curtain coating die, having a narrow slot at its lower face. The slot has a clearance of 0.4 mm, and is 400 mm wide. The die is mounted onto a portal. At both sides of the portal, a tooth belt slide is provided (Isotec CA-80, Austria). The slide span measures 1800 mm. The tooth belts' driving gears are mechanically connected, and driven by a 750 W servo motor (Yaskawa SGMPH-08, Japan), with corresponding amplifier (Yaskawa SGDH-08). The servo amplifier is controlled by a 1.5 axis machine controller (Yaskawa MP940). The controller is needed to execute motion with well-defined acceleration trajectories. The servo motor features a 13 bit incremental encoder.

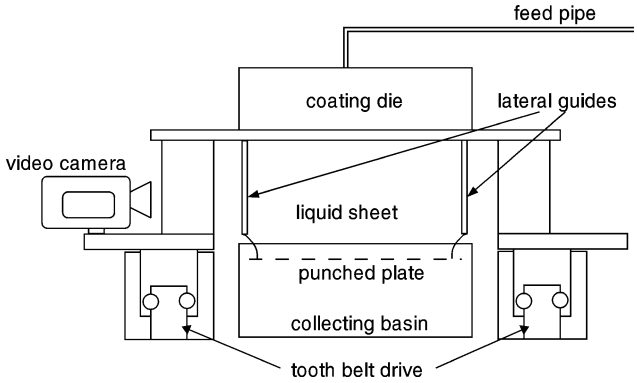

Fig. 1. Front view of the measurement set-up for recording the transient response of a moving liquid sheet.

2.1. Acceleration

Dedicated time-dependent acceleration trajectories $a_D(t)$ were imparted to the coating die. Different kinds of acceleration trajectories were used to investigate how a given acceleration trajectory affects the sheet's transient response. All trajectories were specified with the aim of reaching a desired coating speed V_C after a specified acceleration length AL (distance that the die system has to travel before a constant V_C is reached). The trajectories that were used can be divided into three classes:

- a second degree polynomial trajectory ($P2$-class):

  $$a_{P2}(t) = c_2 t^2 + c_1 t$$

  this trajectory features a discontinuous jerk (derivative of acceleration) at the interval ends ($c_1 \neq 0$);
- a fourth degree polynomial trajectory ($P4$-class):

  $$a_{P4}(t) = c_4 t^4 + c_3 t^3 + c_2 t^2$$

  this trajectory features a continuous jerk all over its interval (values c_i were properly selected);
- a sinusoidal trajectory (S-class):

  $$a_S(t) = c_1 \sin(\omega t + \phi) + c_2$$

  the jerk here is also continuous.

Another characteristic parameter of the acceleration trajectories is the peak acceleration (a_{peak}), which is determined by the acceleration length, the coating speed, and by the trajectory class. Fig. 2 shows the three trajectory classes for a coating speed $V_C = 1\ \text{m s}^{-1}$ and acceleration length $AL = 275$ mm. For a given acceleration length and coating speed, a $P2$-trajectory will have the smallest peak acceleration, a S-trajectory the highest.

Both controller and amplifier were configured such that the actual imparted acceleration trajectories matched the programmed ones. Fig. 3 shows an example of the match between programmed and measured acceleration trajectories. The measured trajectory was extracted from encoder data, while the programmed one is what was input to the controller. The peak acceleration for this trajectory is about $9\ \text{m s}^{-2}$, which is one of the highest performing trajectories used throughout the experiments. The figure shows a satisfactory agreement, and in what follows the programmed trajectories will be considered to be identical to the actual ones. Moreover, in order to make a comparison with numerical simulations, the acceleration trajectories actually imparted to the die have to match the ones used for simulation.

2.2. Extrusion of the sheet

Liquid is fed to the die by a metering gear pump. Control of the pump's rotational speed allows for flow rate control. The sheet, which is extruded out of the die, falls vertically in direction of gravity, over a height of 125 mm. Thereafter it impinges onto a punched plate. When the die is accelerated, the inertia forces will make the sheet bend, as depicted in Fig. 4. At both lateral ends, the liquid sheet is guided by rods (also referred to as edge guides). This is done in order to prevent lateral contraction by surface tension. The liquid remains pinned to these rods even during acceleration, meaning that, at its lateral ends, the sheet does not bend. Thus, deflection is actually 3D, with maximum occurring in the middle. It is the deflection in the middle of the sheet, that is extracted from the video recordings (as shown in Fig. 4).

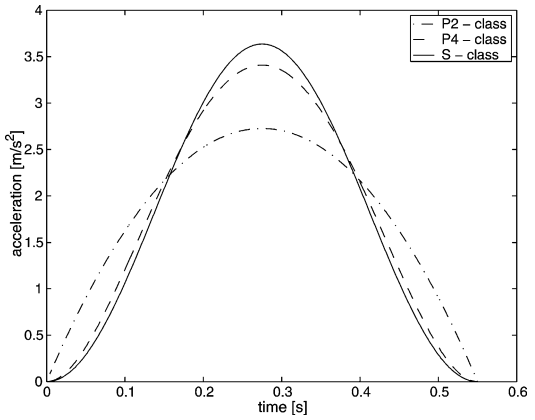

Fig. 2. Comparison between three classes of acceleration trajectories $V_C = 1\ \mathrm{m\,s^{-1}}$, $AL = 275$ mm.

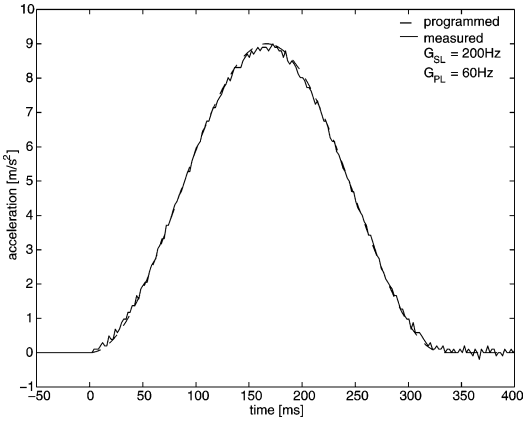

Fig. 3. Comparison between programmed and measured acceleration trajectories: S-class profile, $V_C = 1.5\ \mathrm{m\,s^{-1}}$, $A_L = 250$ mm. G_{SL} is the speed loop gain; G_{PL} is the position loop gain.

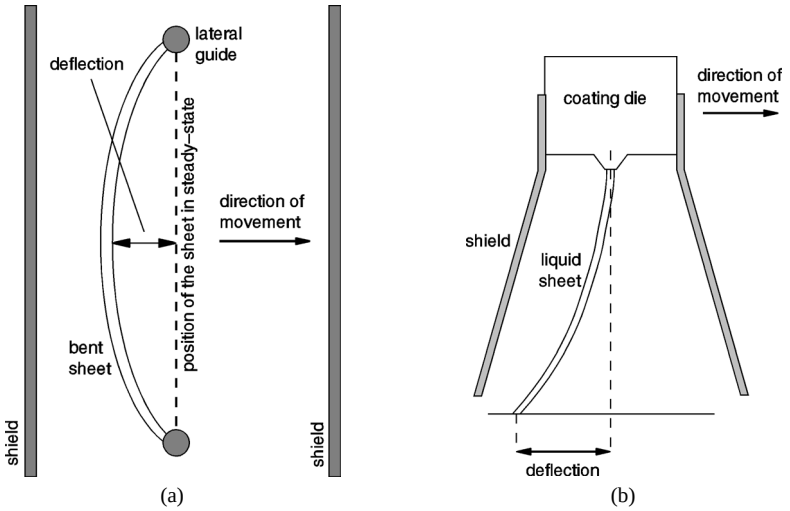

Fig. 4. Schematic representation of the deflection of a liquid sheet when accelerated. The shields are protecting the sheet from aerodynamic influences. (a) Horizontal cross-section of a backwards bent sheet. (b) Vertical cross-section of a backwards bent sheet.

Attention is given to shielding the sheet from surrounding air. Neglect of giving shielding the necessary consideration makes the sheet extremely susceptible to inertia effects of surrounding air when the sheet is moving. This can also be deduced from the derived equations of motion (28) in part I, in which a pressure disturbance of $\mathrm{O}(\varepsilon)$ may cause an O(1) deflection of the sheet. ε is a slenderness ratio. Shields were provided at the sheet's front and back, as depicted in Fig. 4. The clearance between substrate and shield was 1.5 mm. The shields were about 100 mm wider than the sheet. No shielding was provided laterally.

2.3. Procedure

A digital video camera (Sony) is fixed laterally to the portal (see Fig. 1). In this way, the camera moves together with the die, and the liquid sheet. This allows the capturing of clear, sharp images of the sheet's lateral profile. The camera captures 50 frames per second, which is sufficient for the present experiments. The frames captured during motion are processed afterwards to extract deflection information.

In order to allow a quantitative comparison between the various experiments provided in this paper, the out-of-plane deflection at the lower end of the sheet is extracted from the video recordings as quantifiable data. This deflection is measured in the middle between the edge guides, as it is here that deflection is maximal. Fig. 4 illustrates the spot in the sheet where deflection is extracted from the video frames.

For each frame of interest, the elapsed time from motion start has to be known. This is achieved by video recording a LED together with the sheet. When the die is set into motion, this LED will turn on and readily indicates which video frame is given zero time. Thus, the maximum time error on the measurements is less than the interframe period of 20 ms.

The video camera is mounted such that the optical axis is parallel to the sheet (when stationary and planar). By so doing, a video image represents a purely lateral view, and sheet deflection can be easily measured. A calibration is performed beforehand, so as to establish the scale factor. Video images are stored on a digital cassette, and processed afterwards to extract all the frames of interest. Fig. 15(a) shows, as illustration, a sequence of three captured video frames of a bent sheet.

2.4. Liquid properties

The rheology of a liquid can exert a significant influence on the fluid dynamic behaviour. The liquid that was used for the present study is the SOMOS[1] 7100 photopolymer. A sample of this liquid was rheologically characterised at the Department of Chemical Engineering, K.U.Leuven, on a DSR 200 rheometer (Rheometrics). The dynamic viscosity was found to be 1.18 Pa s at 27 °C, and was independent of shear rate (tested up to a shear rate of 100 s^{-1}). The dynamic viscosity was also found to be frequency independent (ratio of loss modulus G'' to frequency ω is constant up to $\omega = 100$ rad s^{-1}). Even though no data is available for higher shear rates, we consider the liquid to be Newtonian.

The static surface tension was measured to be 37 mN m^{-1}. Liquid density $\rho = 1100$ kg m^{-3}. All experiments were performed with a constant flow rate issuing from the die: $Q = 100$ mm^2 s^{-1}. No die swell is observed, and the initial sheet thickness is considered to be equal to the slot clearance: $T_0 = 0.4$ mm. The initial mean streamwise velocity is then easily calculated: $u_0 = Q \cdot T_0^{-1} = 0.25$ m s^{-1}.

3. Experimental results

This section discusses the results that were extracted from the video recordings. Absolute measurement accuracy is ± 2 mm for deflections larger than 5 mm. When deflection gets smaller, the measurement suffers from the presence of the edge guides, around which the sheet thickens due to a smaller velocity. This prevents a clear view of the sheet's lateral shape, and therefore negatively affects accuracy.

Figs. 5–8 present the collected experimental data. The deflection of the sheet is plotted against the distance travelled by the slide system (die and portal). In the figures, this distance is referred to as *die displacement*. It is useful to examine the relation between deflection and die displacement, because it gives an idea of the travel length of the die, required for the transient response to decay. As such, this relation gives a direct indication of the drive span needed for the transient response to decay. An in-depth discussion of the experimental data is provided in what follows.

Fig. 5 introduces a scaling for the deflection data. The figure shows the measured deflection of the sheet for $P4$-class acceleration trajectories and different coating speeds. All trajectories feature an acceleration length $AL = 275$ mm. The deflection, scaled by $V_C^2 g^{-1}$ (g represents the gravitational acceleration), is plotted against the displacement of the die, which is scaled by the coating speed V_C, and has now the unit of time. With the introduced scales, the deflection plots for $V_C = 0.5$ and 0.75 m s^{-1} interestingly collapse. For higher coating speeds, however, the coincidence is lost, and we may state that deflection is less than proportional to V_C^2 for $V_C \geqslant 1$ m s^{-1}. On the other hand, the die displacement needed for the transient response to decay scales with V_C, and holds for $V_C > 1$ m s^{-1}, as Figs. 7 and 8 evidence.

3.1. Influence of the acceleration trajectory class

Fig. 6 shows deflection plots of the sheet's response to different acceleration trajectory classes ($P2$, $P4$, or S), but with identical V_C and AL. The graph shows no significant difference in the responses to the three acceleration classes. The differences in peak acceleration affect the maximal sheet deflection in a minor way.

Fig. 7 shows measured sheet deflections when accelerated to a coating speed $V_C = 1$ m s^{-1}, by S-class trajectories with different acceleration lengths (peak accelerations of 3.6, 5, and 10 m s^{-2}). The responses are plotted against the die displacement scaled by the coating speed, and the figure clearly shows that all three responses need about the same die displacement to decay. The acceleration length, AL, clearly affects the magnitude of deflection. A shorter AL (i.e. higher peak acceleration) increases the magnitude of deflection. Fig. 7 also shows that the drive length needed for the response to decay is a few times AL. Figs. 6 and 7 lead us to conclude that neither the acceleration trajectory class, nor the acceleration length visibly affect the settling time (or settling distance).

[1] Somos is a registered trademark of DSM Desotech.

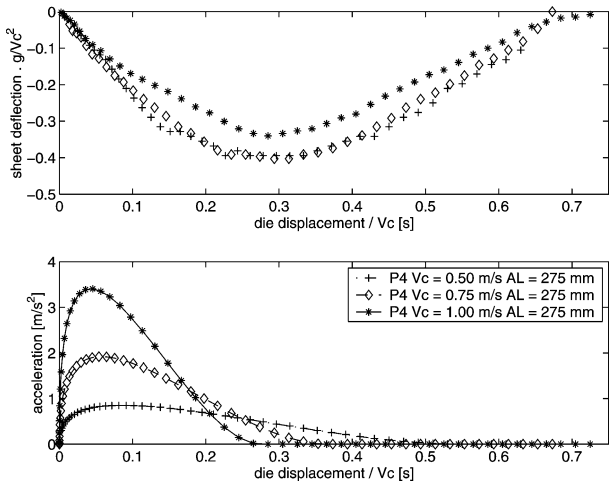

Fig. 5. Sheet deflection during acceleration to three different coating speeds $V_C = 0.50$, 0.75, 1.00 $\mathrm{m\,s^{-1}}$. All acceleration trajectories are $P4$-class, with $AL = 275$ mm. Deflection is scaled by $V_C^2 \cdot g^{-1}$. Die displacement is scaled by V_C. The upper window plots deflection against displacement of the die. Lower window plots the acceleration trajectories.

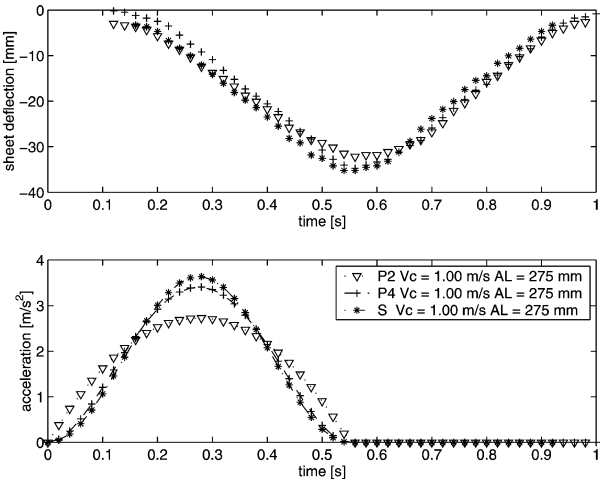

Fig. 6. Experimental responses to different classes of acceleration trajectories. $V_C = 1\ \mathrm{m\,s^{-1}}$, $AL = 275$ mm. The lower graph plots the acceleration trajectories in function of time. The upper graph plots the corresponding sheet's responses.

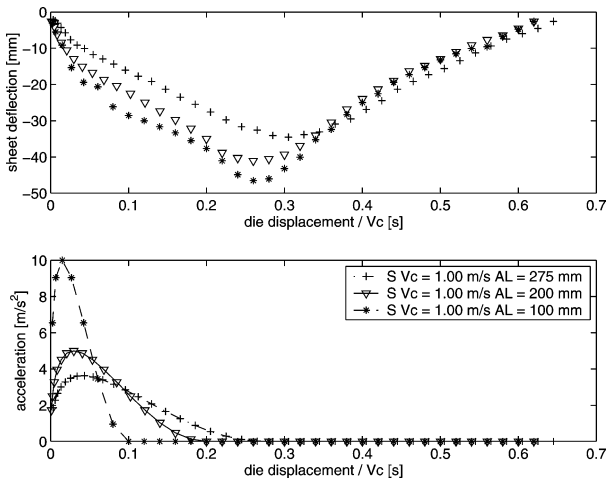

Fig. 7. Experimental responses to S-class acceleration trajectories. $V_C = 1\ \mathrm{m\,s^{-1}}$, $AL = 275$, 200, and 100 mm. The lower graph plots the acceleration trajectories in function of the scaled die displacement. The upper graph plots the corresponding sheet's responses.

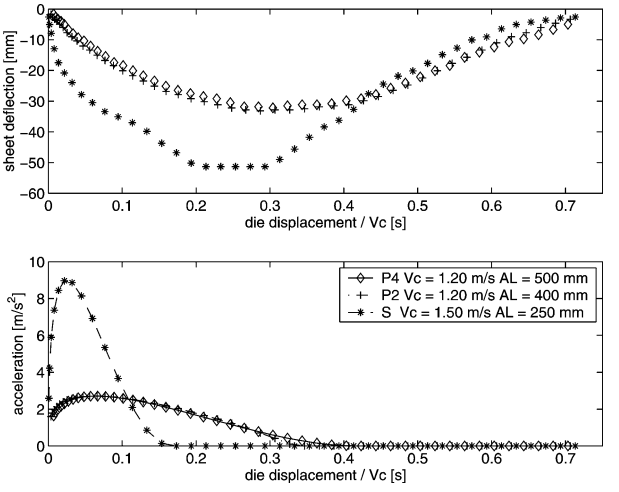

Fig. 8. Experimental responses to different acceleration trajectories. $V_C = 1.2$ and 1.5 $\mathrm{m\,s^{-1}}$. The lower graph plots the acceleration trajectories in function of the scaled die displacement. The upper graph plots the corresponding sheet's responses.

When increasing coating speed beyond 1 $\mathrm{m\,s^{-1}}$, the acceleration trajectories will exhibit larger acceleration lengths or/and higher peak accelerations. This results in larger sheet deflections. The die displacements needed for the responses to decay remain more or less on the order of magnitude of 0.7 V_C. Fig. 8 shows measured transient responses to acceleration trajectories resulting in coating speeds of $V_C = 1.2$ and 1.5 $\mathrm{m\,s^{-1}}$. The sheet's response to the acceleration to $V_C = 1.5\ \mathrm{m\,s^{-1}}$, shows a flattened extremum. This is due to the fact that the deflection was so large that the sheet touched the shield, and thus could not bend further. Table 1 gives an overview of the relevant response parameters for all tested acceleration trajectories.

Table 1
Summary of characteristic parameters of the sheet's response for different acceleration trajectories. τ_{peak}: time to peak acceleration, ℓ_{max}: maximal sheet deflection, τ_{max}: time to ℓ_{max}, τ_{90}: time for the sheet's response to decay to 10% of its maximal value (10% of ℓ_{max})

Acceleration trajectory					Sheet's response					
Class	V_C ($m\,s^{-1}$)	AL (mm)	a_{peak} ($m\,s^{-2}$)	τ_{peak} (s)	Experimental			Simulation		
					ℓ_{max} (mm)	τ_{max} (s)	τ_{90} (s)	ℓ_{max} (mm)	τ_{max} (s)	τ_{90} (s)
P4	0.50	275	0.85	0.550	10.0	0.81	–	11.4	0.59	1.03
P4	0.75	275	1.92	0.367	23.1	0.64	1.00	27.1	0.42	0.70
P4	1.00	425	2.21	0.425	26.8	0.70	1.10	30.6	0.48	0.80
P4	1.00	350	2.68	0.350	30.8	0.63	1.00	38.3	0.40	0.67
P2	1.00	275	2.73	0.275	32.2	0.54	0.92	44.2	0.35	0.59
P4	1.00	275	3.41	0.275	34.7	0.54	0.91	54.0	0.32	0.54
S	1.00	275	3.64	0.275	35.2	0.53	0.90	60.0	0.33	0.53
S	1.00	200	5.00	0.200	41.0	0.44	0.79	109.9	0.31	0.42
S	1.00	100	10.0	0.100	46.5	0.34	0.68	–	–	–
P4	1.20	500	2.70	0.417	32.2	0.70	–	37.8	0.47	0.79
P2	1.20	400	2.70	0.333	33.2	0.60	1.02	37.4	0.39	0.71

4. Simulation of the transient response of a 2D liquid sheet

This section covers the simulations that have been performed to study the transient dynamics of a liquid sheet subjected to acceleration. In part I of this series of papers, time-dependent equations of motion were derived, governing the deflection of a 2D liquid sheet subjected to acceleration, on the assumptions of a slender sheet, and small Reynolds number. The equations were expressed in a 2D curvilinear noninertial reference frame (s, n), with s following the sheet's centre line, and n normal to s. The s-axis is made to *always* coincide with the sheet's centre line, even when the sheet deflects. To characterise the dynamics, a new velocity term was introduced: the normal (directed along n) velocity f of the sheet's centre line. The f-velocity component, together with the sheet thickness T and streamwise velocity u, constitute a set of three unknowns that characterise the sheet's dynamics. Assuming that the liquid sheet is falling in the direction of gravity, and using $a_D(t)$ as the acceleration that is applied to the die (perpendicular to the direction of gravity), the 2D equations of motion derived in part I are expressed as follows:

Continuity

$$\frac{\partial}{\partial s}(Tu) + \frac{\partial T}{\partial t} = 0, \tag{1}$$

Momentum balance

$$\begin{aligned}
(s)\quad & \frac{\partial u}{\partial t} + u\frac{\partial u}{\partial s} + 2\kappa u f = \cos\theta - \frac{a_D}{g}\sin\theta - \frac{1}{2}\frac{\partial}{\partial s}\{p^{g+} + p^{g-}\} + \frac{1}{R}\left\{4\frac{\partial^2 u}{\partial s^2} + \frac{4}{T}\frac{\partial T}{\partial s}\frac{\partial u}{\partial s} - \kappa^2 u\right\},\\
(n)\quad & \frac{\partial f}{\partial t} + u\frac{\partial f}{\partial s} - f\frac{\partial u}{\partial s} - \kappa(u^2 - f^2)\\
& \qquad = \sin\theta + \frac{a_D}{g}\cos\theta - \frac{1}{\varepsilon T}\{p^{g+} - p^{g-}\} - \frac{1}{T}\frac{2\kappa}{We} - \frac{1}{R}\left\{\frac{1}{T}\frac{\partial T}{\partial s}\kappa u + 3\kappa\frac{\partial u}{\partial s} + u\frac{\partial \kappa}{\partial s} + \frac{\partial \kappa}{\partial t}\right\}.
\end{aligned} \tag{2}$$

Here, ε is the ratio of the initial sheet thickness to the sheet length ($T_0 L^{-1}$). As slender sheets are considered, $\varepsilon \ll 1$. $R = \varepsilon^{-1} Re$ is a modified Reynolds number ($Re = \rho u_s T_0 \mu^{-1}$). $u_s = \sqrt{gL}$ is a velocity scale. We is the Weber number ($\rho u_s^2 T_0 \sigma^{-1}$). κ represents the curvature of the s-axis, and p^g the air pressure at the interface. The accuracy of the set of equations (1) and (2) is $O(\varepsilon)$. With the values used during the experiments of Section 3, $Re = 0.4$ and $We = 14.6$.

Based on the set of 2D equations (1) and (2) a computational finite difference model was developed. A predictor–corrector algorithm was used to solve the finite difference equations for the three unknowns T, u, and f. This is an explicit finite-difference method to solve the equations through a time-marching scheme. It is $O(\Delta s^2)$ accurate in both time and space. Calculations were performed with Matlab™ with a time step of 5.0×10^{-4} s. The sheet was modelled with 50 nodes.

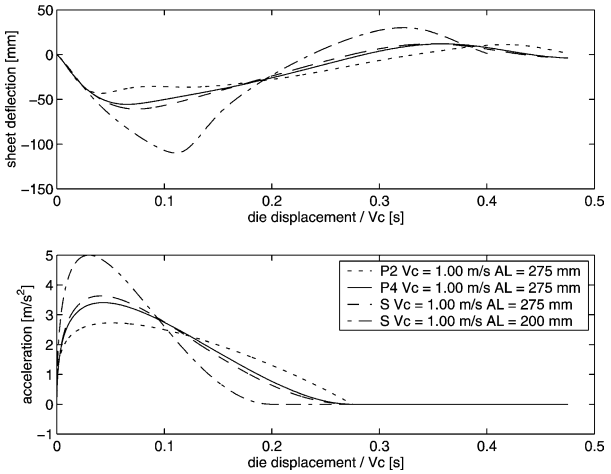

Fig. 9. Simulated sheet's responses to different acceleration trajectories: $P2$ $V_C = 1\ \mathrm{m\,s^{-1}}$, $AL = 275$ mm, $P4$ $V_C = 1\ \mathrm{m\,s^{-1}}$, $AL = 275$ mm, S $V_C = 1\ \mathrm{m\,s^{-1}}$, $AL = 275$ mm, S $V_C = 1\ \mathrm{m\,s^{-1}}$, $AL = 200$ mm. $Q = 100\ \mathrm{mm^2\,s^{-1}}$, $Re = 0.4$. The lower graph plots the acceleration trajectories in function of scaled die displacement. The upper graph plots the corresponding sheet's responses.

A constant feed $Q = u_0 T_0$ is assumed. No pressure differences are present across the sheet: $p^{g+} - p^{g-} \equiv 0$. No downstream solution is specified where the sheet impinges onto the substrate. This last consideration stems from the fact that, when inertia forces dominate the flow, no information can travel upstream the sheet.[2]

4.1. Simulation results

As with the experimental results, the computed responses are represented by the sheet's deflection defined as in Fig. 4. The acceleration trajectories used for the computations are identical to the ones used for the experiments.

Fig. 9 plots the computed responses to different acceleration trajectories, all leading to a coating speed $V_C = 1\ \mathrm{m\,s^{-1}}$. The results are plotted using the same scaling as for the experiments, to ease comparison with the experimental results of Figs. 6 and 7.

The agreement of the computed responses of Fig. 9 with the experimental observed ones in Figs. 6 and 7, for corresponding acceleration trajectories, is however only qualitative. Table 1 summarises the characteristic parameters of the computed responses, and the experiments. The $\ell_{\max}$ and $\tau_{\max}$ data of Table 1 are also presented graphically in Fig. 13, graphs A and C, where the computed values are plotted against the experimental ones. All computed responses feature a larger maximal deflection $\ell_{\max}$, but also faster dynamics ($\tau_{\max}$ and τ_{90}). The computed $\ell_{\max}$ shows an exponential increasing discrepancy with experiment, while the difference between computed and experimental $\tau_{\max}$ is more or less steady for the range under investigation.

Analysis of the discrepancy between experiments and simulations lead the authors to believe that these are due to the dynamics of the air trapped between the sheet and the shields protecting the curtain. The simulations presented up to now have neglected the influence of surrounding air. In the following section the model is empirically modified to include the effect of surrounding air flow.

5. Influence of shielding

The computed responses shown in the previous section show a similar behaviour with the experimental ones, but the agreement is merely qualitative. In general it may be stated that the computations show a faster sheet dynamics for all acceleration trajectories under investigation. Two facts may be identified, which might – at first sight – cause the simulations to disagree with the experiments. A first fact is the 3D behaviour of the liquid sheet used for the experiments. The width to length aspect ratio is 400 to 125 mm, or 3.2, and the computational model of the sheet was 2D. However, experiments have been performed, with the sheet unsupported by edge guides. By so doing, the sheet's lateral ends were free to bend, and the behaviour might

[2] We refer to Lin [8] who showed that in a viscous curtain sinuous waves can propagate upstream only when the *local* Weber number defined by $\rho Q u \sigma^{-1}$ is smaller than 2. At the downstream location of the sheet used for the experiments the local Weber number is 4.4.

better approach the 2D case. In this case the sheet contracted laterally, and at its downstream location measured 280 mm wide. These experiments showed no significant difference in the sheet's response (measured in the sheet's middle), compared to the presented experiments with edge guides. This fact supports the assumption that the sheet's behaviour may well be represented by a 2D model. A second fact is the neglect of the dynamics of the air in the *chambers* between the sheet and the two shields. When the sheet bends, the chambers change in volume. This volume change will have two effects: (i) a change in air pressure, and (ii) an air flow to level the pressure difference between chamber and surroundings through the chamber's lateral open ends (see Fig. 4). The authors conjecture that (i) and (ii) account for additional stiffness and damping effects on the sheet's behaviour. What follows is an attempt to prove this conjecture.

5.1. Facts that support the conjecture

The parameter through which the air surrounding the sheet interacts with the sheet itself, is the air pressure p^g, being dependent on time and space. Sheet deformation and air pressure are strictly coupled, as was evidenced by Schmid and Henningson [9]. They performed a stability analysis of a falling liquid sheet enclosing an air cushion at one side. Using an optimal superposition of low-frequency modes, a strong correlation was found between the pressure signal in the cushion and the fall time of particles in the sheet. The main deformation of the sheet and the pressure signal in the air cushion are caused by wave packets travelling down the sheet, which in turn are triggered due to a global coupling by the compressible air cushion. The correlation could be observed over a wide range of parameters governing the flow, and was in accordance with experimental data.

Finnicum et al. [10] investigated the steady-state deflection of sheets when a pressure difference is applied. A 100 mm deflection was reported for a sheet, 250 mm long and with $Re = 11$, when a pressure difference of only 0.76 Pa was applied. Their experimental results showed good agreement with theoretical predictions.

Experimental evidence of the large influence of the shielding configuration on the transient response is given in Fig. 10. This figure shows two measured sheet's responses to an identical acceleration trajectory, but for two different shielding configurations. A first configuration featured the shields mounted at a distance of 40 mm from the sheet (average distance, due to the shields' oblique shapes – see Fig. 4), while the second configuration had the same shields mounted at 80 mm from the sheet. The second configuration results in a larger maximal deflection, but the time to the maximum is less compared to the first configuration.

In the following section an empirical model is derived governing the effect of surrounding air on the dynamics of the sheet. It is based on an analogy of the sheet's responses with the responses of a mechanical mass-spring-damper system.

5.2. Simulation with added damping

A closer look at the plotted experimental and computed responses of Figs. 6, 7, and 9 shows that the computed and observed responses show qualitatively a similar behaviour. Both approach the response of a second order system. Therefore, consider, by way of illustration, a mechanical second order system, as depicted in Fig. 11. The system consists of a small mass (the sheet), able to move without friction on a cart (the die). The mass is attached to the cart through a spring with stiffness k, and damper

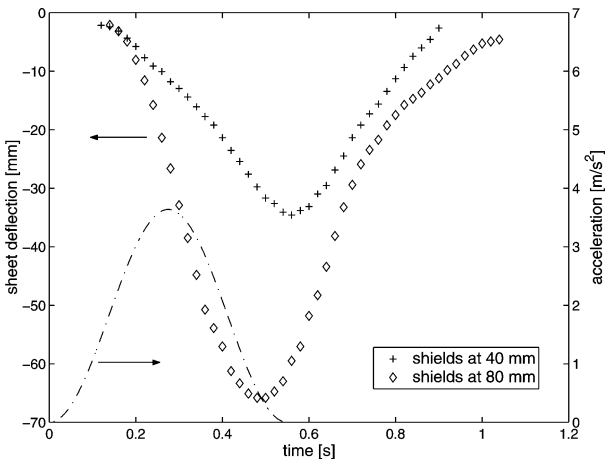

Fig. 10. Experimental responses for two different shielding configurations: (+) shields mounted at 40 mm from sheet, (◇) shields mounted at 80 mm from sheet. Acceleration trajectory: S-class, $V_C = 1\ \mathrm{m\,s^{-1}}$, $AL = 275$ mm.

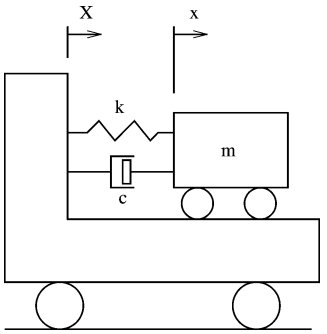

Fig. 11. Simplified mass-spring-damper model of the deflection of a liquid sheet. The mass m coincides with the sheet; the cart is the die imparting the acceleration.

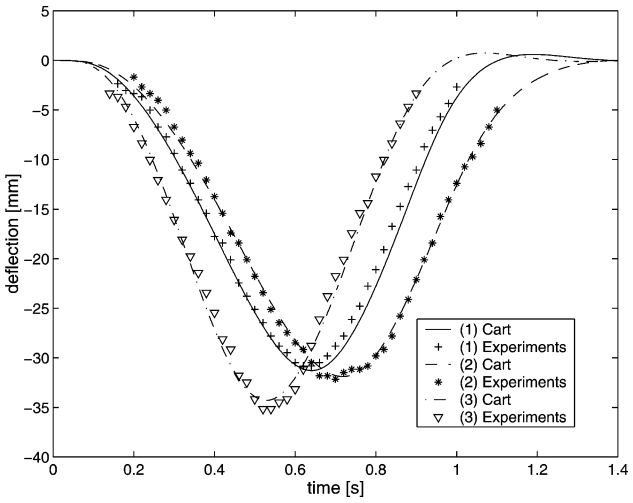

Fig. 12. Match of the responses of the system (3) with measured sheet deflections: (1) $P4$ $V_C = 1\ \mathrm{m\,s^{-1}}$, $AL = 350$ mm, $\zeta = 0.5(1 + 12|\dot{\xi}| - 89|\dot{\xi}|^2)$, $\omega_n = 13.7(1 - 19|\xi| + 40|\xi|^2)$; (2) $P4$ $V_C = 1.2\ \mathrm{m\,s^{-1}}$, $AL = 500$ mm, $\zeta = 0.7(1 + 10|\dot{\xi}| - 92|\dot{\xi}|^2)$, $\omega_n = 12.9(1 - 17|\xi| + 33|\xi|^2)$; (3) S $V_C = 1\ \mathrm{m\,s^{-1}}$, $AL = 275$ mm, $\zeta = 0.5(1 + 10|\dot{\xi}| - 47|\dot{\xi}|^2)$, $\omega_n = 14.7(1 - 19|\xi| + 30|\xi|^2)$.

with coefficient c. The stiffness k of this model corresponds to both the stiffness of the liquid sheet itself, and the stiffness imparted to the sheet by the air trapped in the chambers between sheet and shields. The damper, in the cart model, actually represents the damping influence of the air flow on the sheet's dynamic behaviour. The internal damping of the liquid sheet is neglected.[3]

When the cart is accelerated, the following equation governs the relative motion of the small mass w.r.t. the cart:

$$\ddot{\xi} + 2\zeta\omega_n\dot{\xi} + \omega_n^2\xi = -\ddot{X}, \tag{3}$$

where the dot represents differentiation w.r.t. time, and $\xi = x - X$. The damping ratio $\zeta = c(2\sqrt{mk})^{-1}$ and the natural frequency $\omega_n = \sqrt{km^{-1}}$. The solution of (3) may be fitted to the sheet's measured responses to extract important information on the conjectured damping phenomenon. However, before proceeding to do this, let us note that damping will be highly nonlinear. Therefore, we consider ζ to be a function of the displacement velocity $\dot{\xi}$:

$$\zeta = \zeta^*(1 + \alpha_1|\dot{\xi}| + \alpha_2\dot{\xi}^2). \tag{4}$$

Moreover, the sheet's stiffness will be dependent on the deflection of the sheet, thus, on the displacement ξ:

$$\omega_n = \omega_n^*\big(1 + \kappa_1|\xi| + \kappa_2\xi^2\big). \tag{5}$$

The solution of the second order system (3), expanded with (4) and (5), has been fitted to each measured sheet's response separately. The solutions of the cart model match the sheet's experimental responses quite well, provided that ζ and ω_n are well-chosen. Fig. 12 shows a few matches of experimental responses and fitted solutions of the cart model (3). The numerical values of ζ and ω_n, averaged over all responses, were found to be:

$$\begin{aligned} \zeta &= 0.5\big(1 + 10|\dot{\xi}| - 50\dot{\xi}^2\big), \\ \omega_n &= 13\big(1 - 20|\xi| + 40\xi^2\big). \end{aligned} \tag{6}$$

The value of ω_n^* may also be found by numerical simulation of the equations of motion (2) as follows. A continuous sinuous acceleration is applied to the sheet: $a_D(t) = A\sin\omega t$, and its response is computed according to the method outlined in Section 4. Assuming the system to be undamped ($c = 0$), then the steady state response will also be a sine, with equal frequency, but with a phase shift. The amplitude of the response is $A \cdot (m(\omega_n^2 - \omega^2))^{-1}$. As the sheet's mass can be calculated,

[3] The contribution of viscous forces to the deflection is thus neglected. See part I for a discussion on the influence of viscosity on sheet deflection.

Table 2
Summary of characteristic parameters of the sheet's response for different acceleration trajectories: experimental and computed with damping. τ_{peak}: time to peak acceleration, ℓ_{max}: maximal sheet deflection, τ_{max}: time to ℓ_{max}, τ_{90}: time for the sheet's response to decay to 10% of its maximal value (10% of ℓ_{max}), $\delta\ell_{max} = (\ell_{max,sim} - \ell_{max,exp})/\ell_{max,exp}$, $\delta\tau_{max} = (\tau_{max,sim} - \tau_{max,exp})/\tau_{max,exp}$

Acceleration trajectory			Sheet's response							
Class	V_C ($m\,s^{-1}$)	AL (mm)	Experimental			Sim. w. damp.				
			ℓ_{max} (mm)	τ_{max} (s)	τ_{90} (s)	ℓ_{max} (mm)	$\delta\ell_{max}$ (%)	τ_{max} (s)	$\delta\tau_{max}$ (%)	τ_{90} (s)
P4	0.50	275	10.0	0.81	–	10.0	0.0	0.74	−8.6	–
P4	0.75	275	23.1	0.64	1.00	21.0	−9.1	0.58	−9.4	0.96
P4	1.00	425	26.8	0.70	1.10	25.2	−6.0	0.64	−8.6	1.07
P4	1.00	350	30.8	0.63	1.00	28.8	−6.5	0.59	−6.3	0.94
P2	1.00	275	32.2	0.54	0.92	30.9	−4.0	0.50	−7.4	0.88
P4	1.00	275	34.7	0.54	0.91	31.1	−10.3	0.53	−1.8	0.91
S	1.00	275	35.2	0.53	0.90	31.1	−11.6	0.54	+1.9	0.84
S	1.00	200	41.0	0.44	0.79	31.7	−22.7	0.45	+2.3	0.75
P4	1.20	500	32.2	0.70	–	31.0	−3.7	0.64	−8.5	1.07
P2	1.20	400	33.2	0.60	1.02	32.0	−3.6	0.56	−6.6	0.97

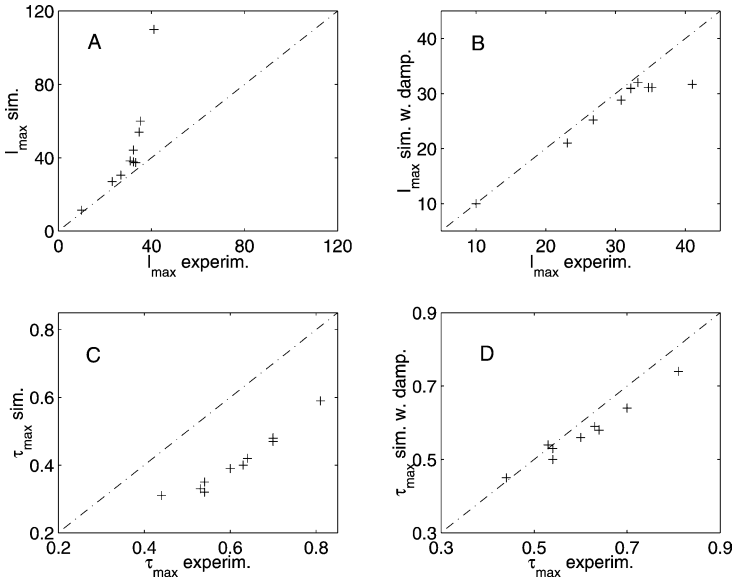

Fig. 13. Plots of ℓ_{max} and τ_{max} data of Tables 1 and 2. Computed values are plotted against experimental ones. Graphs A and C match the values of simulations with *no* damping with experiments. Graphs B and D match the values of simulations *with* damping with experiments.

computation of the response results in $\omega_n^* = 12.5\ rad\,s^{-1}$, which is in good agreement with the value found by curve fitting in (6), and supports the assumptions that (i) the contribution of the air in the chambers to the sheet's stiffness is small, and (ii) the computational model, described in Section 4 is a good estimate of the real sheet. Concerning the damping ratio ζ, a value of $\zeta^* = 0.5$ is considerably high. As previously outlined, this damping cannot stem from the sheet itself, but is caused by the air flow in the chambers. Such a high damping is not present in the computational model of Section 4, which explains the discrepancy between experiments and computational results.

The previous discussion makes clear that a relation of the kind (4) is missing in the computational model of Section 4, while a relation (5) is already included, and no additional stiffness, stemming from the air in the chambers, is needed. Thus, adding a damping term of the form (4) to the equations of motion, should result in a better agreement of the computational results with experiments. The (n)-balance of the momentum equations (2) may then be written as:

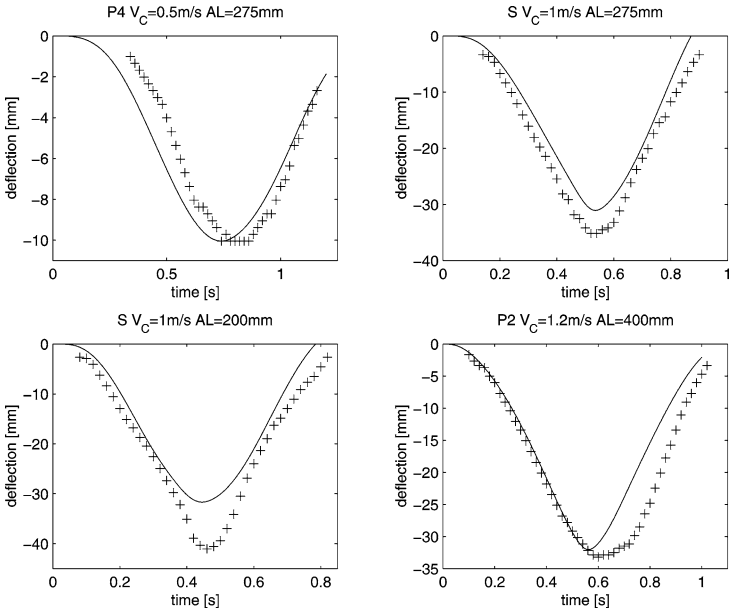

Fig. 14. Comparison between computed responses with damping and experiments. Solid lines represent simulation results; '+' represents experimental data.

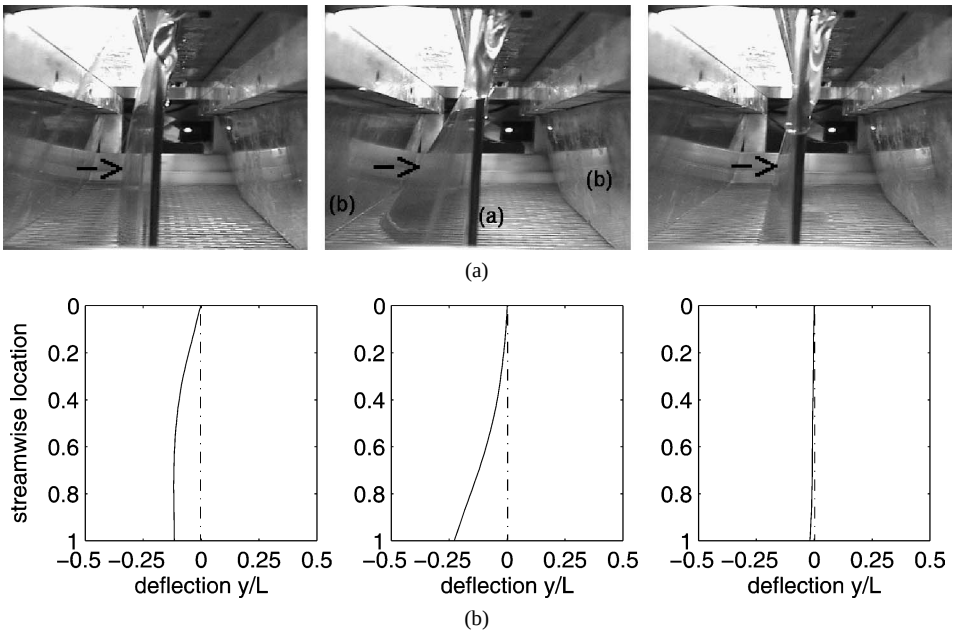

Fig. 15. Video images and computed lateral profiles of a liquid sheet. Acceleration trajectory: S-class, $V_C = 1\ \mathrm{m\,s^{-1}}$, $AL = 275$ mm. Left images: 320 ms after motion start, central images: 600 ms, right images: 880 ms. (a) Sequence of three captured images of a bent sheet. The arrows indicate the bent sheet. (a): edge guide; (b): shields. (b) Computed lateral profiles.

$$\frac{\partial f}{\partial t} + u\frac{\partial f}{\partial s} - f\frac{\partial u}{\partial s} - \kappa(u^2 - f^2) = \sin\theta + \frac{a_D}{g}\cos\theta - \frac{1}{T}\frac{2\kappa}{We} - 2\zeta^*\overline{\omega}_n^*\left\{1 + \overline{\alpha_1}|f| + \overline{\alpha_2}|f|^2\right\}SF(s)f$$
$$- \frac{1}{R}\left\{\frac{1}{T}\frac{\partial T}{\partial s}\kappa u + 3\kappa\frac{\partial u}{\partial s} + u\frac{\partial \kappa}{\partial s} + \frac{\partial \kappa}{\partial t}\right\} \tag{7}$$

with $\overline{\omega}_n^*$, $\overline{\alpha_1}$, and $\overline{\alpha_2}$ the dimensionless counterparts of ω_n^*, α_1, and α_2. $SF(s)$ is a scale factor, linearly scaling the damping influence over the sheet's height. The damping effect is assumed to be highest downstream, and lowest at the die outlet. As depicted in Fig. 4, the shields do not run parallel to the sheet (assuming the sheet to be stationary), but diverge downwards. The scale factor evolves in the same way as the distance between sheet and shield, going linearly from a minimum of 0.65 at the die outlet to a maximum of 1.35 at the substrate.

Solutions of the adapted model (7) – with nonlinear damping – have been computed for various acceleration trajectories. For all computations, the values for ζ^*, ω_n^*, α_1, and α_2 were identical and taken from (6). Table 2 summarises the characteristic response parameters of the simulations with added damping, and compares them with experiments. The agreement between computed responses and experiments is significantly improved, compared with the simulations without damping. This may also be seen from Fig. 13, comparing the computed and experimental $\ell_{\max}$ and $\tau_{\max}$ data graphically. Fig. 14 plots a few responses and compares with experiments. The figure shows clearly that during the stage of increasing deflection, the agreement between simulation and experiments is quite good. The fact that the computed maximal deflection is smaller than the experimental maximum in most of the cases, makes the stage of decreasing deflection not agree well between simulation and experiment. In some cases the computed responses show an overshoot, but this is not experimentally observed, perhaps due to its small magnitude. Fig. 15 compares a sequence of three video images of the deflected sheet with the computed lateral profiles of the sheet, for the same acceleration trajectory, and at the same instants of time. The lateral profiles match well, giving additional validity to the performed simulations.

Let us note that all computations were performed with the same damping coefficients of (6). These coefficients have been empirically obtained. The fact that one damping relationship gives similar results for various trajectories, supports the assumption that the physical mechanism causing damping is the same for all investigated cases. However, Fig. 13 evidences an increasing discrepancy for the trajectories causing the largest deflections (i.e. the trajectories with the highest peak accelerations). This may point out that the damping behaviour of the air alters when the base frequency of the exciting inertia force (i.e. the acceleration trajectory) increases.

6. Conclusion

The transient response of a liquid sheet, subjected to horizontal acceleration of the die from which it emanates, has been measured experimentally for various acceleration trajectories. The measured responses show a very weak dependence on the trajectory class. The acceleration length, and accordingly the peak acceleration only significantly affect the maximal deflection, but merely affect the settling time. Moreover, it has been shown that the shielding of the sheet from surrounding air has a very large impact on the sheet's response.

Comparison of the observed responses with simulations shows that in reality the sheet's response is highly damped. The damping stems from the air flow between sheet and shields, and its characteristic was identified by fitting solutions of a mechanical second order system to the experimental data. The damping ratio was found to be $\zeta = 0.5$, and damping was found to be nonlinear and dependent on the rate of deflection of the sheet.

To improve the agreement between experiments and simulations, a nonlinear damping term was added to the computational model. The resulting computations of the sheet's response show satisfactory agreement with experiments. However, the exact mechanisms that lie at the basis of these damping phenomena are yet unquantifiable and are matter of future research.

Acknowledgements

Part of this research was supported by a research grant from the Flemish Institute for the Promotion of Innovation through Science and Technology (I.W.T.).

The authors would like to express their gratitude to the anonymous referees for their useful comments and suggestions, which have helped improve the paper.

References

[1] L. De Luca, Experimental investigation of the global instability of plane sheet flows, J. Fluid Mech. 399 (1999) 355–376.
[2] L.D. Söderberg, P.H. Alfredsson, Experimental and theoretical stability investigations of plane liquid sheets, Eur. J. Mech. B Fluids 17 (5) (1998) 689–737.
[3] S.P. Lin, Z.W. Lian, B.J. Creighton, Absolute and convective instability of a liquid sheet, J. Fluid Mech. 220 (1990) 673–689.
[4] S.F. Kistler, P.M. Schweizer, Liquid Film Coating – Scientific Principles and Their Technological Implications, Chapman & Hall, 1997.

[5] S.J. Weinstein, K.J. Ruschak, Coating flows, Annu. Rev. Fluid Mech. 36 (2004) 29–53.
[6] S.J. Weinstein, A. Clarke, A.G. Moon, E.A. Simister, Time-dependent equations governing the shape of a two-dimensional liquid curtain, part 1: theory, Phys. Fluids 9 (12) (1997) 3625–3636.
[7] A. Clarke, S.J. Weinstein, A.G. Moon, E.A. Simister, Time-dependent equations governing the shape of a two-dimensional liquid curtain, part 2: experiment, Phys. Fluids 9 (12) (1997) 3637–3644.
[8] S.P. Lin, Stability of a viscous liquid curtain, J. Fluid Mech. 104 (1981) 111–118.
[9] P.J. Schmid, D.S. Henningson, On the stability of a falling liquid curtain, J. Fluid Mech. 463 (2002) 163–171.
[10] D.S. Finnicum, S.J. Weinstein, K.J. Ruschak, The effect of applied pressure on the shape of a two-dimensional liquid curtain falling under the influence of gravity, J. Fluid Mech. 255 (1993) 647–665.